8 Particle Physics at DESY/HERA (H1)

K. Müller, K. Nowak, P. Robmann, U. Straumann, and P. Truöl

in collaboration with:
C. Grab and T. Zimmermann, Institut für Teilchenphysik der ETH, Zürich, S. Egli, M. Hildebrandt, and R. Horisberger, Paul Scherrer Institut, Villigen, and 38 institutes outside Switzerland

(H1 - Collaboration)

The analysis of the data taken by the H1 experiment during 15 years of running is still ongoing. Many analyses were completed using the full data set with an integrated luminosity of 183 pb^{-1} for collisions with electrons and 291 pb^{-1} for collisions with positrons. In addition, first analyses are published which combine the measurements of H1 and ZEUS (1; 2). The deep insight into the structure of the proton at very small distances which result from the precise measurements of H1 and ZEUS has a major impact on the LHC experiments. The final months of HERA operation were devoted to collisions at lower proton energies: 6.2 pb^{-1} and 12.4 pb^{-1} were collected with 27.4 GeV positrons colliding with 575 or 460 GeV protons, respectively. This data has been used for a first direct measurement of the longitudinal structure function F_L, an analysis which was presented for an extended kinematical range at last years conferences.

Fourteen publications (1-14) and several contributions to the 2009 Europhysics Conference on High Energy Physics in Krakow (15,16,18-23) resulted from the continuing effort in the analysis of the H1 data. New results, partly preliminary (24), concern the following topics:

- Direct measurement of the longitudinal structure function F_L in an extended range of Q^2 (19) and for diffractive events (21).

- Precise determination of the neutral electroweak current cross sections over a large range of Q^2 as well as the extraction of the parton density functions (PDF) (1; 12; 14) and the extraction of the charm and beauty contribution to the proton structure function (3; 7).

- Determination of the running coupling constant α_s in jet production (11; 15).

- Production of ρ, K^{*0} and ϕ-mesons (16) and prompt photons (4) at very low Q^2 (photoproduction).

- Final combined analysis of multi-lepton production (6) and production of isolated leptons with large missing momentum (2).

- Search for states and interactions outside the Standard Model (SM), such as single top production (9), excited quarks (10) or squarks (18).

- Measurement of the cross sections and hadronic final state of diffractive events (16; 20; 21; 22)

In the past years our analysis effort concentrated on events with isolated photons produced in either photoproduction ($Q^2 \approx 0$) (25),(26), shortly discussed below (Sec. 8.3), or deep inelastic scattering (DIS, $Q^2 > 4$ GeV^2) (27),(28). Both analyses are finished and have been published. They have been presented in detail in previous annual reports (29). Our involvement in the analysis of prompt photons will continue though with emphasis on less isolated photons (Katharina Müller). One of us (Peter Truöl) continues to serve as referee in the heavy flavour working group.

8.1 Measurement of the longitudinal structure function F_L

The inclusive neutral current DIS cross section at low Q^2 can be written in its reduced form as

$$\begin{aligned}\sigma_r &= \frac{d^2\sigma}{dxdQ^2} \times \frac{Q^4 x}{2\pi\alpha(1+(1-y)^2)} \\ &= F_2(x,Q^2) - \frac{y^2}{1+(1-y)^2} F_L(x,Q^2)\end{aligned} \quad (8.2)$$

Here, y is the inelasticity of the scattering process. The cross section is determined by two independent structure functions F_L and F_2 which are related to the $\gamma^* p$ absorption cross sections of longitudinally and transversely polarised photons, σ_L and σ_T, according to $F_2 \propto (\sigma_L + \sigma_T)$ and $F_2 \propto \sigma_L$. In the Quark Parton Model the value of F_L is zero since longitudinally polarised photons do not couple to spin 1/2 quarks. In Quantum Chromodynamics (QCD) F_L differs from zero due to the presence of gluons in the proton. In the so called DGLAP approximation of perturbative QCD at lowest order F_L is given by

$$F_L = \frac{\alpha_s}{4\pi} x^2 \int_x^1 \frac{dz}{z} [\frac{16}{3} F_2(z) + 8\Sigma e_q^2 (1 - \frac{x}{z}) z g(z)].$$

At low x, F_L directly determines the gluon density in the proton, which is only constrained indirectly by the Q^2 evolution of $F_2(x,Q^2)$. As it is evident from 8.2, the structure functions F_L and F_2 can be extracted by fitting a straight line to σ_r as a function of $y^2/(1+(1-y^2))$. A measurement of DIS cross sections at fixed x and Q^2 but different inelasticities y was achieved at HERA by varying the proton beam energy from nominal 920 GeV to 575 and 460 GeV, while keeping the positron beam energy constant. In these low energy runs a dedicated trigger was used to efficiently trigger the energy depositions with a threshold of 2 GeV. At small energies the trigger was complemented by the CIP2k (31) trigger, developed at our institute. A first direct measurement of the longitudinal structure function F_L was published in 2008 (32). New analyses, presented below, extend the kinematic range probed by the published measurement in four-momentum transfer squared $5 < Q^2 < 800$ GeV and Bjorken x (19) and extract F_L in diffractive events (21).

The sensitivity to F_L is largest at high y as its contribution is proportional to y^2. The kinematic variables x,y and Q^2 are determined from the energy E'_e and polar angle Θ_e of the scattered positron. At low Q^2, high y values correspond to low values of the scattered positron energy. At low energies also hadronic final state particles may mimic an positron signal leading to high background, mainly by photoproduction (γp) processes at $Q^2 \simeq 0$ GeV^2. Removal of the γp background contribution is the major challenge of the measurement of F_L. Part of the γp events are uniquely identified by detecting the scattered positron in tagging calorimeters close to the beampipe downstream of the positron beam. This measurement can be used to tune the simulation of the background. A further method uses the charge symmetry of the background. The charge of the positron candidate is determined from the curvature of the track associated to the positron. Besides small corrections, energy deposits from γp processes are charge symmetric. The wrong charge signal is then used to statistically subtract the background.

Figure 8.1 shows the longitudinal cross sections at low Q^2 as a function of Q^2 at their average x value, it significantly extends the kinematic range of the published measurement (32) ($12 < Q^2 < 90$ GeV^2). The measurement clearly differs from zero and is described by the NLO predictions based on the parton density functions from the H1 fit. For $Q^2 > 10$ GeV^2, the measurement is well described by the NLO H1 fit (30), whereas at low Q^2 the perturbative QCD calculation underestimates the measurement. Dipole models (33; 34) are found to describe the data well. For the entire Q^2 range the measurement is consistent with a value of $R \simeq F_L/(F_L + F_2) = 0.25$.

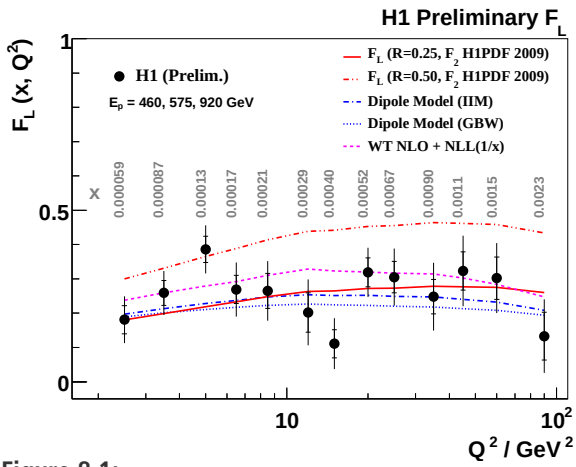

Figure 8.1:
Longitudinal cross section F_L at low Q^2 as a function of Q^2 at their average x value. The curves represent the predictions of a perturbative a QCD calculation at next-to-leading order (NLO) using the H1 PDF 2009 [30] as well as a dipole model [33; 34].

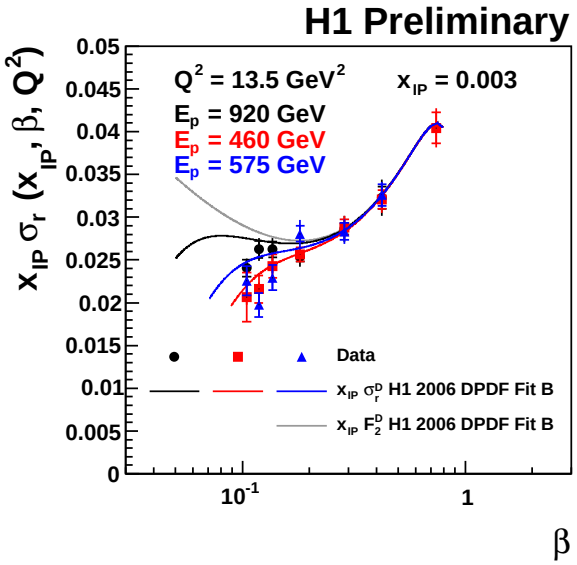

Figure 8.2: Reduced diffractive cross section at E_p= 460, 575 and 920 GeV, the inner error bars are statistical, the outer error bars show the statistical and systematic errors added in quadrature. The cross sections are normalised at 0.28< β <0.42 where the effect of F_L^D is negligible.

For the first measurement of the longitudinal diffractive structure function F_L^D a similar strategy as for the F_L analysis is adopted. In diffraction, the hadronic state system is separated from the scattered proton by a gap that can be observed by the lack of response in the forward parts of the H1 detector (rapidity gap method). The accuracy of this method depends strongly on the understanding of the noise level of the detectors involved.

The data are analysed in the kinematic region $Q^2 > 7$ GeV^2 and $y < 0.9$. Figure 8.2 shows the differential cross section for all three proton beam energies at $7 < Q^2 < 32$ GeV^2 and $0.001 < x_{IP} < 0.01$ as a function of β. Here, $\beta = Q^2/(Q^2+M_X^2)$ and $x_{IP} = (Q^2+M_X^2)/(Q^2+W^2)$, where M_X is the mass of the diffractive system and W the invariant mass of the gamma-proton system. The figure shows also the analytical prediction for σ_r^D to illustrate the effect of the longitudinal structure function. The reduced cross section drops at low β depending on the factor $y^2/(1+(1-y)^2)$ which differs for the three beam energies. The resulting F_L^D measurement is shown in figure 8.3 for four different values of β. The result is compatible with the H1 2006 fit of the diffractive parton density functions (35). Hence, the measurement fully supports the concept of QCD factorisation in diffraction and is an important test of the understanding of the nature of diffractive processes.

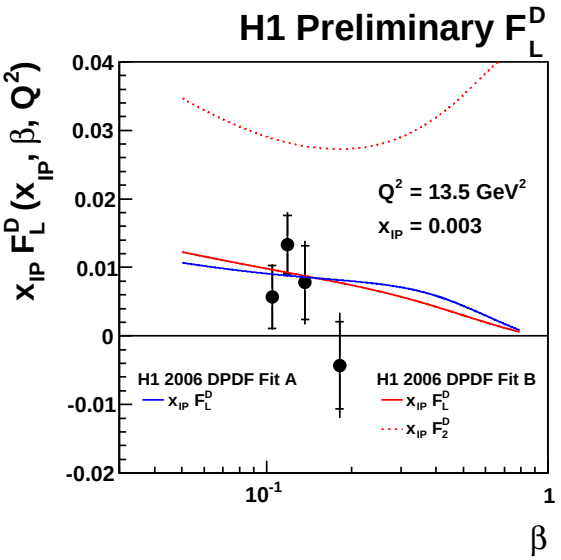

Figure 8.3: Longitudinal diffractive cross section F_L^D compared to the H1 2006 DPDF fits.

8.2 Multiple interactions in photoproduction

Multiple parton interactions (MIA), also referred to as underlying event, play an important role both in electron proton scattering at HERA and even more in high energy proton proton collisions at the TeVatron or the LHC. There,the underlying event is an important element of the hadronic environment within which all physics at the LHC, from Higgs searches to physics beyond the standard model, will take place. In order to tune the Monte Carlo models it is important to measure as many aspects of multiple interactions as possible.

In quasi-real photoproduction ($Q^2 \simeq 0$) the photon has a point-like as well as a hadronic (resolved) component. The transition from a point-like photon to a hadronic object can be studied at HERA as a function of x_γ, the momentum fraction of the parton from the photon which takes part in the hard interaction. Multiple or multi-parton interactions are expected for resolved photons ($x_\gamma < 1$) but not for point-like photons ($x_\gamma \simeq 1$). In photoproduction at HERA the underlying event is studied in di-jet events. The underlying event is defined as everything except the lowest order process (two jets). Besides contributions from higher order QCD radiation and hadronisation it receives also contributions from multi-parton interactions.

Figure 8.4 shows the charged particle multiplicity as a function of the azimuth, where the leading jet is by definition at $\Phi = 180°$, for a resolved photon enriched ($x_\gamma < 0.7$) sample. The data are compared to predictions from PYTHIA. The inclusion of multiple interactions clearly improves the description in the region transverse to the jet ($60° < \Delta\Phi < 120°$ and $240° < \Delta\Phi < 300°$). as well as in the toward ($120° < \Delta\Phi < 240°$) and away ($300° < \Delta\Phi < 60°$) regions, where it contributes as a pedestal to the track multiplicity.

Figure 8.5 shows the average charge multiplicity in the region of the jet P_T^{Jet1} with the highest transverse momentum for $x_\gamma < 0.7$. The track multiplicity rises with P_T^{Jet1}. While the distribution for $x_\gamma > 0.7$ (not shown here), which contains only one hard interaction, is reasonably well described by the simulation, this is clearly not enough to describe the distribution in the resolved enriched sample, especially at lower values of P_T^{Jet1}. Including multi-parton interactions brings the prediction

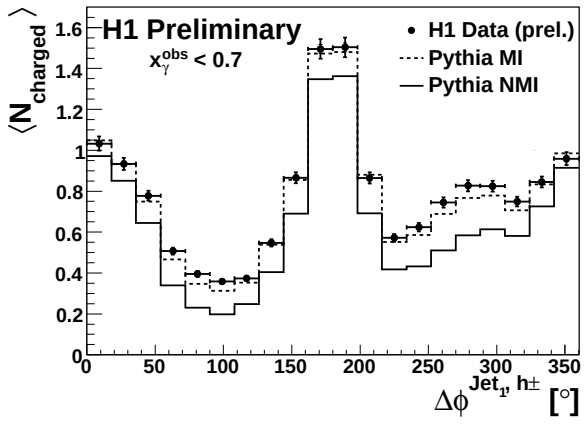

Figure 8.4: Charged particle multiplicity for $x_\gamma < 0.7$. The leading jet axis is by definition at $\Phi = 180°$. The data is compared to PYTHIA with and without multiple interactions.

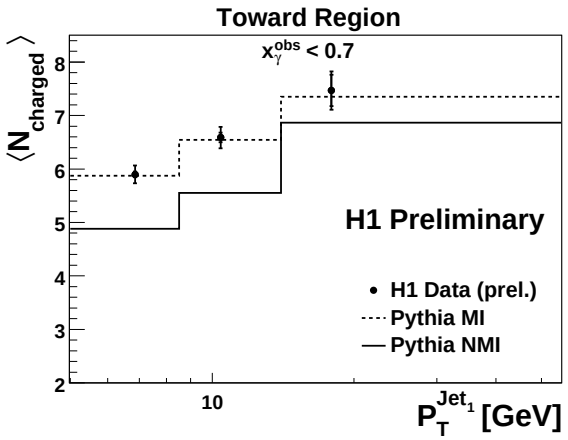

Figure 8.5:
Charged particle multiplicity for $x_\gamma < 0.7$ in the region close to the leading jet. The data is compared to PYTHIA with and without multiple interactions.

in good agreement with the measurement. In the region transverse to the leading jet the average charged particle multiplicity ranges between 0.5 to 2.5 particles, almost independent of P_T^{Jet1}. Again, the region of $x_\gamma > 0.7$ is reasonably well described without including MIA, whereas the region of $x_\gamma < 0.7$ requires multiple interactions to be included. In regions where the photon develops a hadronic structure this measurement fully supports the picture of multi-parton interactions as observed at the TeVatron (36).

8.3 Photon analysis

Isolated photons have been in the focus of our group for the past few years, the effort resulted in two publications (25; 27) and two completed PHD thesis (26; 28). The analysis of isolated photon emerging from the hard subprocess $ep \to e\gamma X$ - so called prompt photons - in photoproduction (PhD thesis of Krzysztof Nowak) was finished during last year. The analysis is based on events at very low Q^2 with the scattered electron escaping detection through the beam pipe and an isolated photon. The data collected during 2004-2007 correspond to a total integrated luminosity of 340 pb^{-1}, three times the value of the previous measurement. Isolated photons with transverse energy $6 < E_T^\gamma < 15$ GeV and pseudo-rapidity $-1.0 < \eta^\gamma < 2.4$ are selected in events with inelasticity $0.1 < y < 0.7$. To ensure isolation of the photon, the energy fraction z of the photon-jet carried by the photon candidate has to to be larger than 90% ($z \equiv E^\gamma / E^{photon-jet} > 0.9$). The isolation rejects a large part from the background from decay photons of neutral hadrons in dijet photoproduction events. The photon signal is extracted by combining different shower shape variables into a discriminator. A novel method, based on a regularised unfolding procedure (37; 38), was developed for this analysis to simultaneously unfold the cross section and determine the fraction of signal and background. Final results of the analysis have been shown in last years report. Overall it was shown that QCD calculations based on the collinear factorisation in NLO (39; 40) or the k_T factorisation approach (41) underestimate the cross section at low transverse momenta of the photon (E_T^γ) and that they are not able to fully describe the transverse correlations between the photon and the jet. The transverse correlations are particularly sensitive to the fraction of resolved events in the sample and to higher order effects. It was therefore studied whether the description of the data by the models could be improved by increasing the intrinsic transverse momentum $< k_T >$ of the partons in the proton which could mimic higher order gluon radiation. Figure 8.6 shows the cross section as a function of the transverse correlation between the jet and the photon for the sample in which direct interactions are enhanced ($x_\gamma > 0.8$). Two variables are defined: $p_\perp$, the transverse momentum of the photon perpendicular to the jet direction and $\Delta\Phi$ the azimuthal difference. The measurement is compared to a NLO prediction (39; 40) which has no intrinsic $< k_T >$ and clearly under-

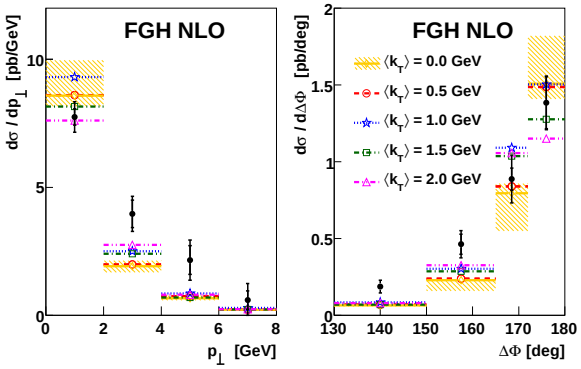

Figure 8.6:
Cross sections for prompt photons in photoproduction with $x_\gamma > 0.7$ as a function of $p_\perp$, the transverse momentum of the photon perpendicular to the jet direction and $\Delta\Phi$ the azimuthal difference. The measurement is compared to a NLO prediction [39; 40] with different assumptions on the intrinsic transverse momentum of the partons in the proton.

estimates the tails. With increasing $< k_T >$ the description of the tails improves, though the last bin in $\Delta\Phi$ remains low. Our studies in this field will continue by analysing less isolated photons which may be used to extract the quark to photon fragmentation function.

[1] F. D. Aaron *et al.* [H1/ZEUS], JHEP **1001** (2010) 109.

[2] F. D. Aaron *et al.* [H1/ZEUS], JHEP **1003** (2010) 035.

[3] F. D. Aaron *et al.* [H1], Phys. Lett. **B 686** (2010) 91.

[4] F. D. Aaron *et al.* [H1], Eur. Phys. J. C **66** (2010) 17.

[5] F. D. Aaron *et al.* [H1], Phys. Lett. B **681** (2009) 391.

[6] F. D. Aaron *et al.* [H1/ZEUS], JHEP **0910** (2009) 013.

[7] F. D. Aaron *et al.* [H1], Eur. Phys. J. C **65** (2010) 89.

[8] F. D. Aaron *et al.* [H1], Phys. Lett. B **681** (2009) 125.

[9] F. D. Aaron *et al.* [H1], Phys. Lett. B **678** (2009) 450.

[10] F. D. Aaron *et al.* [H1], Phys. Lett. B **678** (2009) 335.

[11] F. D. Aaron *et al.* [H1], Eur. Phys. J. C **65** (2010) 363.

[12] F. D. Aaron *et al.* [H1], Eur. Phys. J. C **64** (2009) 561.

[13] F. D. Aaron *et al.* [H1], Phys. Lett. B **673** (2009) 119.

[14] F. D. Aaron *et al.* [H1], Eur. Phys. J. C **63** (2009) 625.

[15] F. D. Aaron *et al.* [H1], Eur. Phys. J. C **67** (2010) 1.

[16] F. D. Aaron *et al.* [H1], JHEP **1005** (2010) 032.

[17] Contributed papers by the H1-Coll. to EPS2009, the 2009 Europhysics Conference on High Energy Physics, Krakow, 16-22 July, 2009; only papers are listed, which are not yet submitted to journals.

[18] **Search for Squark Production in R-Parity Violating Supersymmetry at HERA** [17].

[19] **Measurement of the Longitudinal Structure Function F_L of the Proton at Low x in an extended Q^2 range** [17].

[20] **Diffractive photoproduction of jets with the H1 detector** [17].

[21] **Measurement of the diffractive longitudinal structure function F_L^D at HERA II** [17].

[22] **Measurement of diffractive deep-inelastic scattering with a leading proton at HERA-2** [17].

[23] **A Measurement of the Pomeron Trajectory based on Elastic Rho Photoproduction** [17].

[24] Preliminary H1 results to be presented at the 2010 Workshop on Deep Inelastic Scattering (DIS 2010), Florence, April 19-23, 2010, *http://www-h1.desy.de/publications/H1preliminary.short_list.html*.

[25] F. D. Aaron *et al.* [H1], Eur. Phys. J. C **66** (2010) 17.

[26] **Prompt photon production in photoproducion at HERA**, Krzysztof Nowak, PhD Thesis, University of Zürich (2009) http://www-h1.desy.de/publications/theses_list.html.

[27] F. D. Aaron *et al.* [H1], Eur. Phys. J. C **54** (2008) 371.

[28] **Isolated photon production in deep-inelastic scattering at HERA**, Carsten Schmitz, PhD Thesis, University of Zürich (2007) http://www-h1.desy.de/publications/theses_list.html.

[29] Physik-Institut, University of Zürich, Annual Reports 1996/7 ff.; available at *http://www.physik.unizh.ch/reports.html*.

[30] C. Adloff *et al.* [H1], Eur. Phys. J. C **30** (2003) 1.

[31] J. Becker *et al.*, Nucl. Instrum. Meth. A **586** (2008) 190.

[32] F. D. Aaron *et al.* [H1], Phys. Lett. **B 665** (2008) 138.

[33] K. Golec-Biernat and M. Wüsthoff, Phys. Rev. D **59** (1999) 014017.

[34] E. Iancu, K. Itakura and S. Munier, Phys. Lett. **B 590** (2004) 199.

[35] A. Aktas *et al.* [H1], Eur. Phys. J. C **48** (2006) 715.

[36] A. A. Affolder *et al.* [CDF], Phys. Rev. D **65** (2002) 092002.

[37] V. Blobel, "An unfolding method for high energy physics experiments," Proc. Advanced Statistical Techniques in Particle Physics, Durham (2002).

[38] R. Brun and F. Rademakers, Nucl. Instrum. Meth. A **389** (1997) 81, Version 5.22 was used.

[39] M. Fontannaz, J. P. Guillet and G. Heinrich, Eur. Phys. J. C **21** (2001) 303.

[40] M. Fontannaz and G. Heinrich, Eur. Phys. J. C **34** (2004) 191.

[41] A.V. Lipatov and N.P. Zotov, Phys. Rev. D **72** (2005) 054002.